INTERNATIONAL JOURNAL FOR NUMERICAL METHODS IN FLUIDS
*Int. J. Numer. Meth. Fluids* 2008; **57**:1171–1187
Published online 14 April 2008 in Wiley InterScience (www.interscience.wiley.com). DOI: 10.1002/fld.1807

# An artificial-dissipation-based fractional step scheme for upper-convected Maxwell (UCM) fluid flow past a circular cylinder

C.-B. Liu and P. Nithiarasu*, †

*School of Engineering, Swansea University, Swansea SA2 8PP, U.K.*

SUMMARY

The fully explicit characteristic-based split (CBS) scheme is employed to solve viscoelastic flow problems. The upper-convected Maxwell (UCM) model is employed in the present study. In addition to allowing equal-order interpolations for pressure and velocity, the proposed method along with an appropriate artificial damping scheme is able to produce stable solutions for different Deborah numbers (*De*). The higher-order time terms introduced by the simplified characteristic Galerkin approximation are sufficient to obtain stable solution at very low *De*, but an additional damping is essential to maintain positive definitiveness of the conformation tensor at higher *De*. We demonstrate the need for an additional damping by analysing the basic forward time central space scheme applied to the constitutive equations. A second-order artificial damping is employed to counteract the negative dissipation introduced by the explicit time discretization. The example studied in this paper is the widely used and difficult problem of flow past a circular cylinder. The results presented show that the velocity and extra stresses converge easily to a steady state at lower *De* values. At higher *De* values, the convergence to steady state is slow due to the incremental way in which the artificial damping is added. Copyright © 2008 John Wiley & Sons, Ltd.

Received 12 February 2008; Revised 12 February 2008; Accepted 21 February 2008

KEY WORDS: CBS scheme; UCM model; artificial dissipation (AD); FEM; fractional step method; incompressible; viscoelastic

## 1. INTRODUCTION

The three major issues of current interest in the numerical modelling of viscoelastic flows are stability, large memory overhead and accuracy. Stability and accuracy are closely linked. The

*Correspondence to: P. Nithiarasu, School of Engineering, Swansea University, Swansea SA2 8PP, U.K.
†E-mail: P.Nithiarasu@swansea.ac.uk

Contract/grant sponsor: Engineering and Physical Sciences Research Council (EPSRC); contract/grant number: EP/C515498/1

memory overhead is the result of solving a number of extra stress component equations. The memory overhead can be reduced via matrix-free solution methods, such as the one used in the present study. The stability and accuracy of many numerical schemes deteriorate as the mesh is refined and the elasticity of the fluid is increased. There are a number of differential-type models available for representing a wide spectrum of viscoelastic fluids. Among the available models, the Oldroyd-B and upper-convected Maxwell (UCM) models are commonly employed and other models such as PTT and Giesekus are gaining popularity. In our previous publications [1, 2], we demonstrated how a matrix-free, artificial-compressibility-based fractional step method can be used to reduce some of the stability problems in using Oldroyd-B model. In addition to reducing instability, we have also demonstrated an improved accuracy of drag prediction by adding artificial damping [2]. A consistent second-order dissipation was used to maintain the positive definitiveness of the conformation tensor up to a Deborah number ($De$) of 2, although steady-state solution was obtained beyond $De=2$. In the present work, we have extended the artificial-compressibility-based fractional step method to solve the more challenging UCM fluid model.

Owing to the lack of diffusion terms in the momentum equation, the UCM model is known to introduce severe stability problems as $De$ is increased [3–7]. Many of the studies reported use structured meshes. In the present work, we have employed three fully unstructured meshes and one hybrid mesh to solve the UCM model for flow past a circular cylinder. However, one of the major objectives in viscoelastic flow calculations is to obtain accurate solutions at as high $De$ as possible. Thus, any attempt that helps to push the $De$ limit further on the fine meshes, without loosing positive definitiveness, should be investigated.

The method based on matrix-logarithm of conformation tensor for transforming constitutive equations has been recently proposed by Fattal and Kupferman [8]. The objective of this method is to design an algorithm that retains positive definitiveness of the conformation tensor and removes the growth of exponential stress profiles at higher Weissenberg numbers. Such a scheme was implemented using the finite element method by Hulsen [9] for viscoelastic flow past a confined circular cylinder using the Oldroyd-B model. Hulsen [9] introduced an extra differential equation to produce a symmetric matrix in the discrete elastic viscous split stress (DEVSS) formulation. An alternative form of logarithm-based method for solving all the governing equations was implemented with DEVSS-TG/SUPG up to a Deborah number of 0.7 [10]. Although the positive definiteness is guaranteed, the accuracy is not always assured [10]. In addition to extra variables, the matrix-logarithm-based method has been demonstrated only on the structured meshes. In the present study, the focus is either unstructured or hybrid mesh.

The stabilization proposed here is different from the classical methods such as SUPG [3, 4, 11, 12] and GLS [5, 13–16]. We use the time-stepping-based stabilization to reduce oscillations due to the Galerkin discretization of first-order terms [17–19]. In addition, we also employ a fractional step to reduce pressure instability (LBB condition) and an artificial compressibility scheme to keep the scheme matrix free [20–26]. This method is referred to as the characteristic-based split (CBS) method and it was employed to tackle Oldroyd-B fluid in References [1, 2].

Although the CBS scheme is conditionally stable for Newtonian fluids [19], the same conditional stability is not valid for differential equations governing the extra stresses of the viscoelastic fluids. This is demonstrated by analysing a simple time discretization of the constitutive equations later. Although the characteristic Galerkin (CG) scheme neutralizes some of the opposite stabilization terms, the simple time discretization used here retains some other negative diffusion terms. To counteract these negative diffusion terms, we may need additional dissipation. We have introduced



DOI: 10.1002/fld

a second-order, positive, additional damping to reduce the influence of these negative diffusion terms [1, 27–30].

In summary, the objective of the present work is to model UCM fluid past a circular cylinder using the CBS scheme and a novel artificial damping method. Section 2 summarizes the governing equations for the UCM model. In Section 3, the CBS scheme, the forward time central space (FTCS) scheme and the artificial dissipation (AD) method are discussed. Numerical solutions obtained for different *De*'s are given in Section 4. Some conclusions are derived in Section 5.

## 2. MATHEMATICAL FORMULATIONS

The non-dimensional, isothermal equations for viscoelastic flows can be expressed as

$$\frac{\partial \mathbf{W}}{\partial t}+\frac{\partial \mathbf{F}_j}{\partial x_j}+\frac{\partial \mathbf{G}_j}{\partial x_j}=0 \tag{1}$$

where

$$\mathbf{W}=\begin{bmatrix}\rho\\ \rho u_1\\ \rho u_2\end{bmatrix},\quad \mathbf{F}_j=\begin{bmatrix}\rho u_j\\ \dfrac{1}{Re}(\delta_{1j}p)+\rho u_1 u_j\\ \dfrac{1}{Re}(\delta_{2j}p)+\rho u_2 u_j\end{bmatrix},\quad \mathbf{G}_j=\begin{bmatrix}0\\ \dfrac{1}{Re}(-\tau^n_{1j}-\tau^p_{1j})\\ \dfrac{1}{Re}(-\tau^n_{2j}-\tau^p_{2j})\end{bmatrix} \tag{2}$$

in which the Newtonian deviatoric stress tensor can be expressed as

$$\tau^n_{ij}=(1-\alpha)\left(\frac{\partial u_i}{\partial x_j}+\frac{\partial u_j}{\partial x_i}-\frac{2}{3}\frac{\partial u_k}{\partial x_k}\delta_{ij}\right) \tag{3}$$

and the non-Newtonian deviatoric stress tensor ($\tau^p_{ij}=\tau^e_{ij}+\tau^v_{ij}$), which is given by the constitutive equation of extra stress for polymer contribution, can be expressed as

$$\tau^e_{ij}=-De\left[\frac{\partial \tau^p_{ij}}{\partial t}+\frac{\partial}{\partial x_k}(u_k\tau^p_{ij})-\tau^p_{ik}\frac{\partial u_j}{\partial x_k}-\tau^p_{jk}\frac{\partial u_i}{\partial x_k}\right] \tag{4}$$

and

$$\tau^v_{ij}=\alpha\left(\frac{\partial u_i}{\partial x_j}+\frac{\partial u_j}{\partial x_i}-\frac{2}{3}\frac{\partial u_k}{\partial x_k}\delta_{ij}\right) \tag{5}$$

In the above governing equations, $p$ is the pressure, $\rho$ is the density, $u_j$ are the velocity components, $\delta_{ij}$ is the Kronecker delta, $\tau^e_{ij}$ is the polymer-contributed elastic stress, $\tau^v_{ij}$ is the polymer-contributed viscous stress, $\alpha=\eta_{m0}/\eta_0$ in which $\eta_{m0}$ represents the polymer-contributed viscosity and $\eta_0$ represents the zero shear rate viscosity, $Re$ is the Reynolds number and $De$ is the Deborah number defined as

$$Re=\frac{\rho_\infty u_\infty L}{\eta_0},\quad De=\frac{\lambda u_\infty}{L} \tag{6}$$



DOI: 10.1002/fld

where subscript $\infty$ indicates a free stream value, $L$ is a characteristic length indicating the radius of a circular cylinder, $\lambda$ is the relaxation time and $\eta_0=\eta_n+\eta_{m0}$ in which $\eta_n$ represents the Newtonian dynamic viscosity. In Equation (4), when $0<\alpha<1$, the constitutive equation describes the Oldroyd-B model and the UCM model is obtained when $\alpha=1$.

## 3. NUMERICAL FORMULATIONS

### *3.1. CBS scheme*

The CBS scheme is based on the simplified CG procedure and a fractional step method [17–19]. In this paper, a fully explicit CBS form [1, 2, 20, 21] has been employed to solve Maxwell fluid flow past a circular cylinder. Following the intermediate momentum at the first step, the pressure is calculated from the modified mass conservation at step 2. The velocity field is corrected at step 3. Finally, the discretized constitutive equations are solved with CG stabilization terms at the fourth step. The first three steps are standard and are available in previously published articles [18, 20–26]. Only the discrete forms of the constitutive equation are discussed here. The semi-discrete form of step 4 is

$$\begin{aligned}
\Delta\tau_{ij}^p &= \tau_{ij}^{p\,n+1}-\tau_{ij}^{p\,n}\\
&= \Delta t\left[-\frac{\partial}{\partial x_k}(u_k\tau_{ij}^p)-\frac{\tau_{ij}^p}{De}\right]^n\\
&\quad+\Delta t\left[\tau_{ik}^p\frac{\partial u_j}{\partial x_k}+\tau_{jk}^p\frac{\partial u_i}{\partial x_k}+\frac{\alpha}{De}\left(\frac{\partial u_i}{\partial x_j}+\frac{\partial u_j}{\partial x_i}-\frac{2}{3}\frac{\partial u_k}{\partial u_k}\delta_{ij}\right)\right]^n\\
&\quad+\frac{(\Delta t)^2}{2}\left\{u_m\frac{\partial}{\partial x_m}\left[\frac{\partial}{\partial x_k}(u_k\tau_{ij}^p)+\frac{\tau_{ij}^p}{De}\right]\right\}^n\\
&\quad+\frac{(\Delta t)^2}{2}\left\{u_m\frac{\partial}{\partial x_m}\left[-\left(\tau_{ik}^p\frac{\partial u_j}{\partial x_k}+\tau_{jk}^p\frac{\partial u_i}{\partial x_k}\right)\right]\right\}^n\\
&\quad+\frac{(\Delta t)^2}{2}\left\{u_m\frac{\partial}{\partial x_m}\left[-\frac{\alpha}{De}\left(\frac{\partial u_i}{\partial x_j}+\frac{\partial u_j}{\partial x_i}-\frac{2}{3}\frac{\partial u_k}{\partial u_k}\delta_{ij}\right)\right]\right\}^n
\end{aligned}\tag{7}$$

In the above equation, the higher-order terms act as a convection-stabilizing mechanism. The CG procedure gives the positive diffusion, which may be expressed in compact form as

$$D_{ij}^+=\frac{\Delta t}{2}\left[u_m\frac{\partial}{\partial x_m}\left(-\frac{\partial\tau_{ij}^p}{\partial t}\right)\right]^n\tag{8}$$



DOI: 10.1002/fld

where the time rate of increasing extra stress is

$$\frac{\partial \tau_{ij}^p}{\partial t} = -\frac{\partial}{\partial x_k}(u_k \tau_{ij}^p) + \tau_{ik}^p \frac{\partial u_j}{\partial x_k} + \tau_{jk}^p \frac{\partial u_i}{\partial x_k} - \frac{\tau_{ij}^p}{De} + \frac{\alpha}{De}\left(\frac{\partial u_i}{\partial x_j} + \frac{\partial u_j}{\partial x_i} - \frac{2}{3}\frac{\partial u_k}{\partial x_k}\delta_{ij}\right) \tag{9}$$

and for the two-dimensional viscoelastic flow problems, we have this in detailed form for each component of the constitutive equation as

$$\begin{aligned} D_{11}^+ &= -\frac{\Delta t}{2}\left[u_1 \frac{\partial}{\partial x_1}\left(\frac{\partial \tau_{11}^p}{\partial t}\right) + u_2 \frac{\partial}{\partial x_2}\left(\frac{\partial \tau_{11}^p}{\partial t}\right)\right]^n \\ D_{12}^+ = D_{21}^+ &= -\frac{\Delta t}{2}\left[u_1 \frac{\partial}{\partial x_1}\left(\frac{\partial \tau_{12}^p}{\partial t}\right) + u_2 \frac{\partial}{\partial x_2}\left(\frac{\partial \tau_{12}^p}{\partial t}\right)\right]^n \\ D_{22}^+ &= -\frac{\Delta t}{2}\left[u_1 \frac{\partial}{\partial x_1}\left(\frac{\partial \tau_{22}^p}{\partial t}\right) + u_2 \frac{\partial}{\partial x_2}\left(\frac{\partial \tau_{22}^p}{\partial t}\right)\right]^n \end{aligned} \tag{10}$$

Applying the standard Galerkin approximation to the semi-discrete form of the equation (Equation 7), the final matrix form of the constitutive equations is obtained as

$$\Delta \underline{\underline{\tilde{\tau}}}^p = -\mathbf{M}_{\tau^p}{}^{-1} \Delta t [(\mathbf{C}_{\tau^p} \underline{\underline{\tilde{\tau}}}^p + \mathbf{K}_{\tau^p} \underline{\underline{\tilde{\tau}}}^p - \mathbf{D}_{\tau^p}) - \Delta t (\mathbf{K}_{\mathbf{s}} \underline{\underline{\tilde{\tau}}}^p + \mathbf{T}_{\mathbf{s}} \underline{\underline{\tilde{\tau}}}^p - \mathbf{D}_{\mathbf{s}})]^n \tag{11}$$

where the extra stress variables are approximated using same-order interpolation functions as velocity and pressure. In the present study, we use linear triangular elements for the spatial discretization of all variables. The matrices in Equation (11) are given as

$$\begin{aligned} \mathbf{M}_{\tau^p} &= \int_\Omega \mathbf{N}_{\tau^p}^{\mathrm{T}} \mathbf{N}_{\tau^p} \,\mathrm{d}\Omega, \quad \mathbf{C}_{\tau^p} = \int_\Omega \mathbf{N}_{\tau^p}^{\mathrm{T}} (\nabla^{\mathrm{T}}(\mathbf{u}\mathbf{N}_{\tau^p}))\,\mathrm{d}\Omega, \quad \mathbf{K}_{\tau^p} = \frac{\mathbf{M}_{\tau^p}}{De} \\ \mathbf{D}_{\tau^p} &= \int_\Omega \mathbf{N}_{\tau^p}^{\mathrm{T}} \left(\underline{\underline{\tilde{\tau}}}^p \nabla \mathbf{N}_{\mathbf{u}} \tilde{u} + \frac{\underline{\underline{\tilde{\tau}}}^v}{De}\right)\mathrm{d}\Omega, \quad \mathbf{K}_{\mathbf{s}} = -\frac{1}{2}\int_\Omega (\nabla^{\mathrm{T}}(\mathbf{u}\mathbf{N}_{\tau^p}))^{\mathrm{T}} (\nabla^{\mathrm{T}}(\mathbf{u}\mathbf{N}_{\tau^p}))\,\mathrm{d}\Omega \\ \mathbf{T}_{\mathbf{s}} &= -\frac{1}{2De}\int_\Omega (\nabla^{\mathrm{T}}(\mathbf{u}\mathbf{N}_{\tau^p}))^{\mathrm{T}} \mathbf{N}_{\tau^p}\,\mathrm{d}\Omega \\ \mathbf{D}_{\mathbf{s}} &= -\frac{1}{2}\int_\Omega (\nabla^{\mathrm{T}}(\mathbf{u}\mathbf{N}_{\tau^p}))^{\mathrm{T}} \left(\underline{\underline{\tilde{\tau}}}^p \nabla \mathbf{N}_{\mathbf{u}} \tilde{u} + \frac{\underline{\underline{\tilde{\tau}}}^v}{De}\right)\mathrm{d}\Omega \end{aligned} \tag{12}$$

### 3.2. FTCS scheme

As the constitutive equations are substantially different from standard convection equations, explaining the negative diffusion generated may be easier using the FTCS scheme. To demonstrate the negative diffusion, the one-dimensional constitutive equation is discretized using the finite-difference-based FTCS scheme as

$$\frac{\tau_l^{p^{n+1}} - \tau_l^{p^n}}{\Delta t} + u_l^n \frac{\tau_{l+1}^{p^n} - \tau_{l-1}^{p^n}}{2\Delta x} - \tau_l^{p^n} \frac{u_{l+1}^n - u_{l-1}^n}{2\Delta x} + \frac{\tau_l^{p^n}}{De} - \frac{4\alpha}{3De}\frac{u_{l+1}^n - u_{l-1}^n}{2\Delta x} = 0 \tag{13}$$



DOI: 10.1002/fld

Substituting the Taylor series expansion into Equation (13), we recover the differential form along with the following negative diffusion terms:

$$D_l^- = -\frac{\Delta t}{2!}\frac{\partial^2 \tau_l^{p^n}}{\partial t^2} - \frac{(\Delta t)^2}{3!}\frac{\partial^3 \tau_l^{p^n}}{\partial t^3} - \frac{(\Delta x)^2}{3!}\left[u_l^n \frac{\partial^3 \tau_l^{p^n}}{\partial x^3} - \left(\tau_l^{p^n} + \frac{4\alpha}{3De}\right)\frac{\partial^3 u_l^n}{\partial x^3}\right] + O(\Delta t^3) \tag{14}$$

Neglecting the third- and higher-order terms and generalizing to multi-dimensions, we obtain

$$D_{ij}^- = -\frac{\Delta t}{2!}\frac{\partial^2 \tau_{ij}^{p^n}}{\partial t^2} \tag{15}$$

For the two-dimensional problems, each component of approximate, negative diffusion may be expressed as (assuming a steady velocity field)

$$\begin{aligned} D_{11}^- = {} & \frac{\Delta t}{2!}\left[u_1 \frac{\partial}{\partial x_1}\left(\frac{\partial \tau_{11}^p}{\partial t}\right) + u_2 \frac{\partial}{\partial x_2}\left(\frac{\partial \tau_{11}^p}{\partial t}\right)\right]^n \\ & + \frac{\Delta t}{2!}\left[\left(\frac{1}{De} - \frac{\partial u_1}{\partial x_1} + \frac{\partial u_2}{\partial x_2}\right)\frac{\partial \tau_{11}^p}{\partial t} - 2\frac{\partial \tau_{12}^p}{\partial t}\frac{\partial u_1}{\partial x_2}\right]^n \\ & + \frac{\Delta t}{2!}\left[\frac{\partial \tau_{11}^p}{\partial x_1}\frac{\partial u_1}{\partial t} + \frac{\partial \tau_{11}^p}{\partial x_2}\frac{\partial u_2}{\partial t} - 2\tau_{12}^p \frac{\partial}{\partial x_2}\left(\frac{\partial u_1}{\partial t}\right)\right]^n \\ & + \frac{\Delta t}{2!}\left[\left(\tau_{11}^p + \frac{2\alpha}{3De}\right)\frac{\partial}{\partial x_2}\left(\frac{\partial u_2}{\partial t}\right) - \left(\tau_{11}^p + \frac{4\alpha}{3De}\right)\frac{\partial}{\partial x_1}\left(\frac{\partial u_1}{\partial t}\right)\right]^n \end{aligned} \tag{16}$$

$$\begin{aligned} D_{12}^- = D_{21}^- & \\ = {} & \frac{\Delta t}{2!}\left[u_1 \frac{\partial}{\partial x_1}\left(\frac{\partial \tau_{12}^p}{\partial t}\right) + u_2 \frac{\partial}{\partial x_2}\left(\frac{\partial \tau_{12}^p}{\partial t}\right)\right]^n \\ & + \frac{\Delta t}{2!}\left[\frac{1}{De}\frac{\partial \tau_{12}^p}{\partial t} - \frac{\partial \tau_{11}^p}{\partial t}\frac{\partial u_2}{\partial x_1} - \frac{\partial \tau_{22}^p}{\partial t}\frac{\partial u_1}{\partial x_2}\right]^n \\ & + \frac{\Delta t}{2!}\left[\frac{\partial \tau_{12}^p}{\partial x_1}\frac{\partial u_1}{\partial t} + \frac{\partial \tau_{12}^p}{\partial x_2}\frac{\partial u_2}{\partial t}\right]^n \\ & + \frac{\Delta t}{2!}\left[-\left(\tau_{22}^p + \frac{\alpha}{De}\right)\frac{\partial}{\partial x_2}\left(\frac{\partial u_1}{\partial t}\right) - \left(\tau_{11}^p + \frac{\alpha}{De}\right)\frac{\partial}{\partial x_1}\left(\frac{\partial u_2}{\partial t}\right)\right]^n \end{aligned} \tag{17}$$



DOI: 10.1002/fld

$$D_{22}^{-}=\frac{\Delta t}{2!}\left[u_1\frac{\partial}{\partial x_1}\left(\frac{\partial\tau_{22}^p}{\partial t}\right)+u_2\frac{\partial}{\partial x_2}\left(\frac{\partial\tau_{22}^p}{\partial t}\right)\right]^n$$
$$+\frac{\Delta t}{2!}\left[\left(\frac{1}{De}-\frac{\partial u_2}{\partial x_2}+\frac{\partial u_1}{\partial x_1}\right)\frac{\partial\tau_{22}^p}{\partial t}-2\frac{\partial\tau_{21}^p}{\partial t}\frac{\partial u_2}{\partial x_1}\right]^n$$
$$+\frac{\Delta t}{2!}\left[\frac{\partial\tau_{22}^p}{\partial x_2}\frac{\partial u_2}{\partial t}+\frac{\partial\tau_{22}^p}{\partial x_1}\frac{\partial u_1}{\partial t}-2\tau_{21}^p\frac{\partial}{\partial x_1}\left(\frac{\partial u_2}{\partial t}\right)\right]^n$$
$$+\frac{\Delta t}{2!}\left[\left(\tau_{22}^p+\frac{2\alpha}{3De}\right)\frac{\partial}{\partial x_1}\left(\frac{\partial u_1}{\partial t}\right)-\left(\tau_{22}^p+\frac{4\alpha}{3De}\right)\frac{\partial}{\partial x_2}\left(\frac{\partial u_2}{\partial t}\right)\right]^n \tag{18}$$

Equations (16)–(18) show clearly that the first two terms of the negative diffusion are equal and opposite to the positive diffusion of the CG method as given in Equation (10). Thus, the CG method is expected to eliminate these two terms. However, the remainder of the negative diffusion terms are retained within the method. A careful investigation of these extra terms shows that some of them are zero (e.g. divergence-free velocity) and others are the function of *De*. This and our previous experiences with the Oldroyd-B model [2] show that inaccuracy and instability builds up as *De* increases. This effect of the negative diffusion may be reduced by employing two different approaches. The first is to add a positive diffusion exactly equal to the negative diffusion, which is retained by the scheme. Although sensible, this approach is extremely expensive due to the addition of many extra terms. The second approach is to add a consistent artificial damping term to the discrete constitutive equations to counteract the negative diffusion. This is a much cheaper approach than the former approach and is thus adopted in the present work. The following subsection gives two artificial damping options.

### *3.3. AD method*

It is well known that, in many situations, adding AD to a scheme can effectively damp the unstable phenomenon and smooth numerical results without destroying the accuracy. In this paper, artificial damping is added to the discrete constitutive equation (Equation (11)). Here, two different methods are proposed. The first dissipation method is based on the difference between consistent and lumped mass matrices, an approximation for second derivatives of the extra stress components [1, 27–30], i.e.

$$\frac{\partial}{\partial x_j}\left(h^2\frac{\partial\tau_{ij}^p}{\partial x_j}\right)x_i\approx\mathbf{M}_{\tau^p}{}^{-1}(\mathbf{M}_{\tau^p}-\mathbf{M}_{\tau^pL})\underline{\underline{\tilde{\tau}}}^p \tag{19}$$

With the addition of this artificial damping, the smoothed extra stress equation becomes

$$\Delta\underline{\underline{\tilde{\tau}}}^p{}_r=\Delta\underline{\underline{\tilde{\tau}}}^p+\Delta t\mathbf{M}_{\tau^p}{}^{-1}\frac{C_eS_e}{\Delta t}(\mathbf{M}_{\tau^p}-\mathbf{M}_{\tau^pL})\underline{\underline{\tilde{\tau}}}^{p\,n} \tag{20}$$

where subscript $r$ indicates a smoothed solution, $\mathbf{M}$ is the mass matrix, subscript $L$ indicates a lumped mass matrix and $S_e$ is an elementally averaged switch of nodal pressure values,



DOI: 10.1002/fld

given as

$$S_i = \frac{\left|\sum_1^n (p_i - p_k)\right|}{\sum_1^n |p_i - p_k|} \tag{21}$$

where $n$ is the number of nodes connected to $i$. In Equation (20), $C_e$ is an artificial damping constant that should be carefully chosen to add an optimal amount of damping, sufficient to eliminate all negative eigenvalues of the conformation matrix within the flow domain. Equation (20) can also be visibly consistent with the original discretization of constitutive equation as the mesh is refined, which means that the element size $h$ in Equation (19) tends to zero.

An alternative method [30] is to directly estimate the second derivative of extra stresses using the post-processed second derivatives of the extra stress components. The smoothed extra stress equation with this second option is

$$\Delta \underline{\underline{\tilde{\tau}}}^p{}_r = \Delta \underline{\underline{\tilde{\tau}}}^p + \Delta t \mathbf{M}_{\tau^p}{}^{-1} C_e h^3 \frac{|\mathbf{u}| + \beta}{\bar{p}} |\nabla^2 p|_e \mathbf{H}_{\tau^p} \underline{\underline{\tilde{\tau}}}^{p\,n} \tag{22}$$

where $\bar{p}$ is the average pressure, $h$ is the local element size, $\beta$ is the artificial wave speed and

$$\mathbf{H}_{\tau^p} = -\int_\Omega (\nabla \mathbf{N}_{\tau^p})^{\mathrm{T}} \nabla \mathbf{N}_{\tau^p} \, \mathrm{d}\Omega \tag{23}$$

In Equation (22), the second derivative of the extra stress is calculated at nodes using a post-processing approach and the mean values are then calculated over each element [19]. In the present study, we present only the numerical results obtained from using the first artificial damping method due to its simplicity and cost effectiveness.

## 4. NUMERICAL EXAMPLE

### *4.1. Domain and boundary conditions*

As shown in Figure 1, a circular cylinder with radius $R$ is placed into a rectangular channel at a distance $12R$ from the inlet. The channel is $28R$ long and the distance from the centre of the cylinder to the channel walls is $2R$. The total height of the channel is $4R$.

Three unstructured meshes and one hybrid mesh are generated with fine elements close to the cylinder surface. Typical element sizes on the cylinder surface are 0.10924, 0.05474, 0.00633 and 0.001, respectively, for the four different meshes generated. The hybrid mesh is automatically generated by growing normals on the cylinder surface. The surface normals are used as guides to place structured layers close to the cylinder surface [31]. The meshes in the vicinity of the cylinder are shown in Figure 2(a)–(d). Figure 3(a) and (b) shows two full grids (second and fourth grids) used in the study. From now onwards, we refer to the unstructured meshes as A, B and C with the finest being C and the coarsest being A. We refer to the fourth as mesh HD (hybrid Delaunay).

At the inlet and exit of the channel, parabolic velocity profiles are assumed, i.e.

$$u_1 = 1.5\left(1 - \frac{x_2^2}{4}\right) \tag{24}$$

$$u_2 = 0 \tag{25}$$



DOI: 10.1002/fld

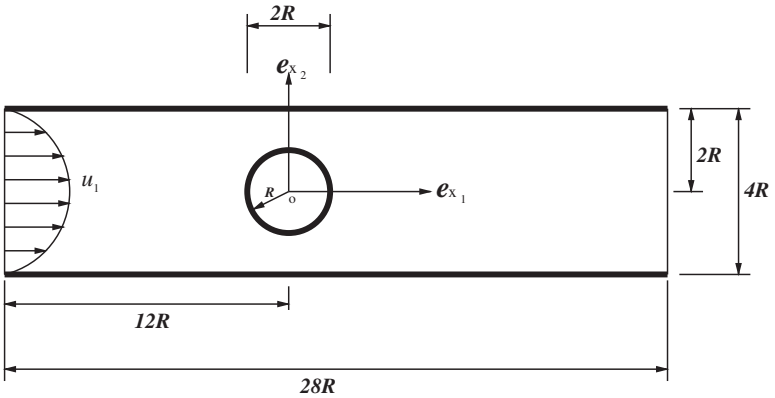


Figure 1. Viscoelastic flow past a circular cylinder placed in a channel.

Consistent with the velocity boundary conditions, the steady distribution of extra stresses at the inlet section is assumed. The stress components are found by analytically solving the constitutive equations at the inlet. The non-dimensional form of the stress distribution at the inlet is given as

$$\tau_{11}^p = 2\alpha De \left(\frac{\partial u_1}{\partial x_2}\right)^2 \tag{26}$$

$$\tau_{12}^p = \alpha \frac{\partial u_1}{\partial x_2} \tag{27}$$

$$\tau_{22}^p = 0 \tag{28}$$

On the channel solid walls and cylinder surface, no slip conditions are assumed. No extra stress conditions are applied on channel walls and the cylinder surface. Both the viscoelastic fluid models are solved without the convection terms in the momentum equation.

### *4.2. Steady-state convergence criterion*

The steady-state convergence criterion is fixed based on the normalized $L_2$ norm of the residual of the equations. It is given as

$$\|e\|_2^{\phi} = \frac{[\sum_{i=1}^{m} (\|\boldsymbol{\phi}\|_i^{n+1} - \|\boldsymbol{\phi}\|_i^{n})^2]^{1/2}}{[\sum_{i=1}^{m} (\|\boldsymbol{\phi}\|_i^{n+1})^2]^{1/2}} \tag{29}$$

where $m$ is the number of nodes in the mesh, $\phi$ indicates the second-order extra stress and velocity components. The above tolerance was reduced to a value of at least $10^{-7}$.

Some sample steady-state convergence histories of the UCM model results are shown in Figure 4. Figure 4(a) and (b) shows the convergence histories at $De = 0.1$ using mesh A. Figure 4(c) and (d) shows the convergence histories at $De = 0.5$ using mesh B. As seen, at $De = 0.1$, mesh A converged quickly to steady state. However, mesh B at $De = 0.5$ took substantially more number of time steps to reach steady state. To accelerate the solution to steady state, we use local time stepping methods



DOI: 10.1002/fld

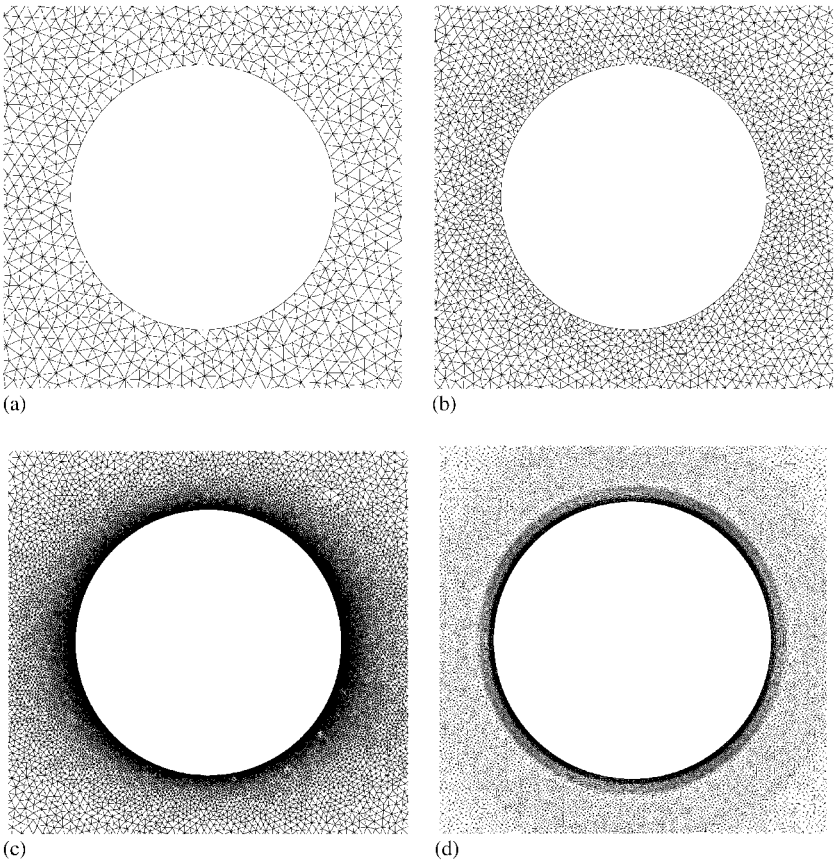


Figure 2. Viscoelastic fluid flow past a circular cylinder. (a) Mesh A (nodes: 13 977; elements: 27 267; $\Delta d = 0.10924$); (b) mesh B (nodes: 16 690; elements: 32 617; $\Delta d = 0.05474$); (c) mesh C (nodes: 33 189; elements: 64 759; $\Delta d = 0.00633$); and (d) hybrid mesh HD (nodes: 35 506; elements: 69 918; $\Delta d = 0.001$).

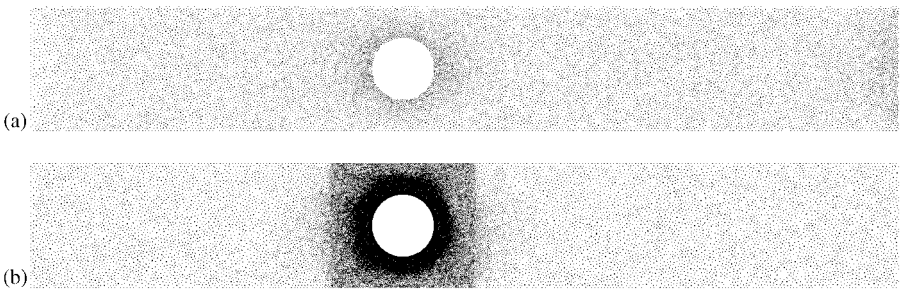


Figure 3. Viscoelastic flow past a circular cylinder. (a) Mesh B and (b) mesh HD.



DOI: 10.1002/fld

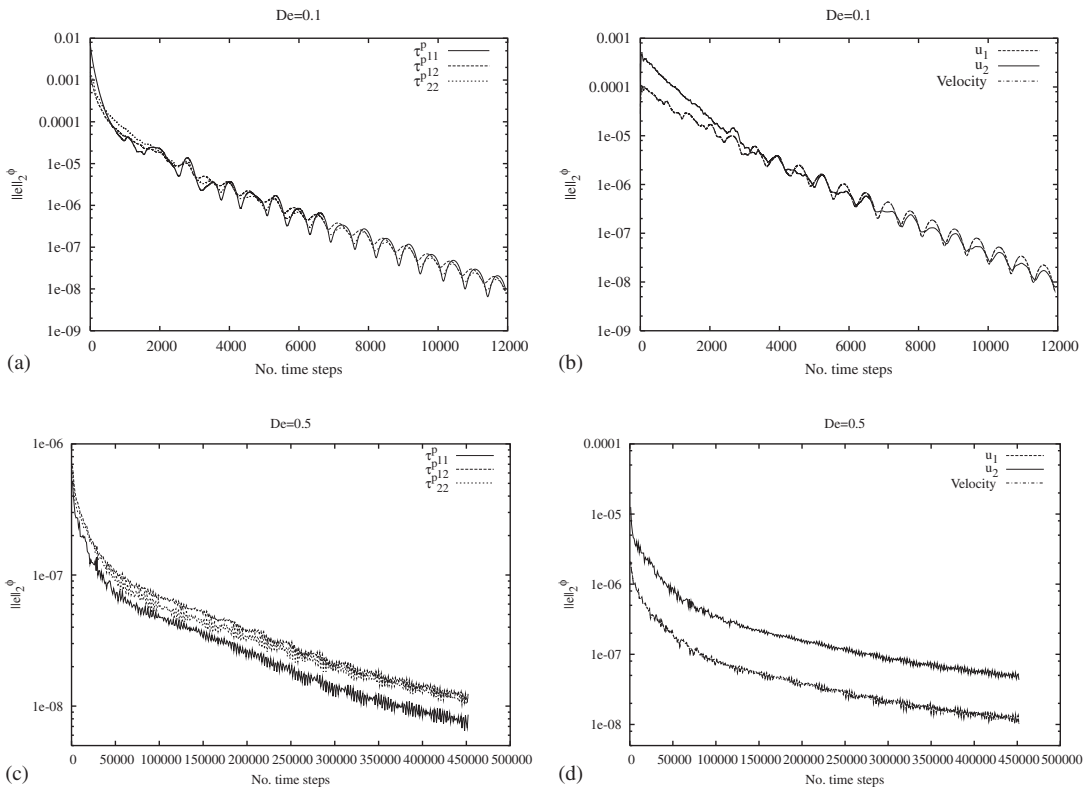


Figure 4. Convergence history of the UCM model, $Re=0.0$.

[1, 2]. At $De=0.1$, the calculation took about 15 min to reach steady state on mesh A and took about 30 min on mesh HD using a standard PC (Intel Pentium 4 CPU 3.00 GHz and 1.00 GB of RAM 2.99 GHz). At highest *De*, for which the results are given, the calculation took about two days. This is due to the incremental variation of artificial damping introduced into the algorithm. We simply stopped calculations if a *De* value took substantially more time than two days.

### *4.3. Results*

To maintain accuracy of the solution, the positive definiteness of the conformation matrix must be maintained throughout the computational field. The positive definiteness of the conformation matrix is also very important for the stability. This is done by making sure that the eigenvalues of the conformation tensor of additional stress are positive [32, 33]. The conformation tensor is given as

$$\tau_{ij}^A = \tau_{ij}^p + (\alpha/De)\delta_{ij} \tag{30}$$

Figure 5 shows eigenvalue contours of the additional stress tensors for the UCM model at $De=0.7$ using mesh HD. As seen, the additional dissipation has not only eliminated negative eigenvalues but also is crucial in obtaining a smooth solution.



DOI: 10.1002/fld

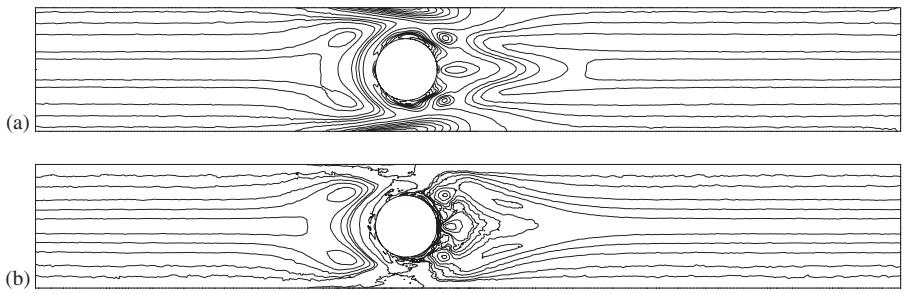


Figure 5. Eigenvalue distribution for the UCM model at $De=0.7$, $Re=0.0$ (mesh HD). (a) $\lambda_1$ contours: $\lambda_{1_{\min}}=1.432$, $\lambda_{1_{\max}}=51.198$ and (b) $\lambda_2$ contours: $\lambda_{2_{\min}}=0.006$, $\lambda_{2_{\max}}=3.817$.

The drag force around the circular cylinder per unit length is calculated in non-dimensional form as

$$D=\int_0^{2\pi}[(-p+\tau_{11}^n+\tau_{11}^p)\cos\theta+(\tau_{12}^n+\tau_{12}^p)\sin\theta]R\,\mathrm{d}\theta \tag{31}$$

In the above equation, both the Newtonian viscous stress components $\tau_{11}^n$ and $\tau_{12}^n$ are zero for the Maxwell fluid employed.

The UCM model is obtained by choosing $\alpha=1$ in the constitutive equations. In all the cases presented, both in this and the following subsections, the steady-state solutions are first obtained without adding artificial damping. We then calculate the eigenvalues at all nodes of the domain. If we find any negative eigenvalue, we add additional damping and converge the solution to steady state. We incrementally increase the additional damping until all the negative eigenvalues are eliminated from the domain.

Figure 6(a) shows the mesh convergence studies carried out using all the four meshes. As seen, we were able to get good mesh convergence up to a Deborah number ($De$) of 0.7. Beyond this value, meshes C and HD took much longer to eliminate negative eigenvalues of the conformation tensor. Thus, we stopped calculations when the time needed for reaching steady state is substantially more than two days.

Figure 6(b) shows the total drag force distribution with respect to $De$. Both meshes A and B are easy to handle up to $De=0.6$ due to a small number of negative eigenvalues appearing in the flow domain without the addition of the artificial damping. Eliminating the small number of negative eigenvalues is relatively easier compared with several hundreds of negative eigenvalues in the field. Beyond $De=0.6$, the drag force produced by mesh A shows an upward trend. This may be the result of additional drag introduced by the artificial damping. When the element sizes are large, it is difficult to control the artificial damping. Larger element sizes, in general, mean larger artificial damping. This is the reason why the drag force produced by mesh A is deviating from its expected path. This shows that although the conformation matrix remains positive definite, the drag force is not necessarily accurate for a given mesh. Mesh B, on the other hand, only shows the effect of extra drag introduced to a much lesser extent. The drag force produced by mesh HD shows a consistent trend in line with other fine mesh results [5, 7]. At $De=0.7$, mesh HD needed elimination of 335 negative eigenvalues around the cylinder. An AD constant value of $C_e=0.064$ is needed to make sure that all negative eigenvalues are removed. Beyond $De=0.7$ the solution on



DOI: 10.1002/fld

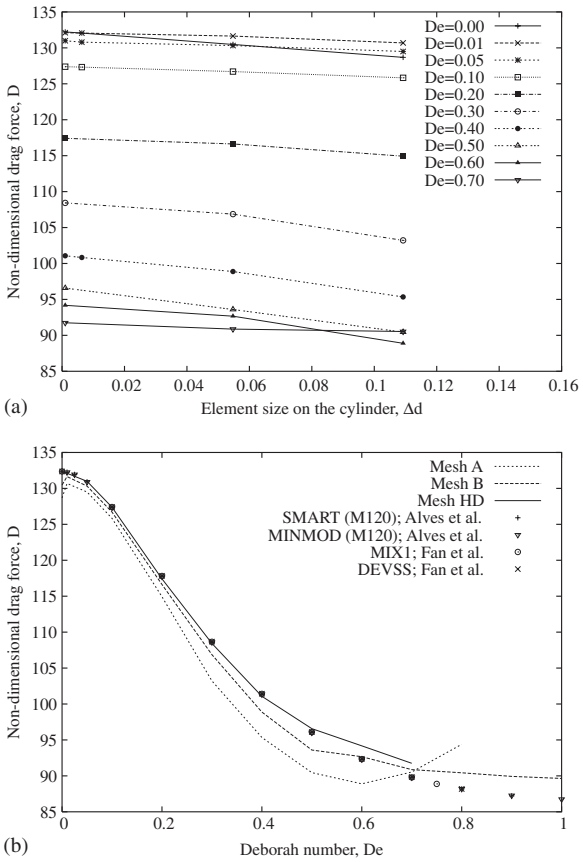


Figure 6. Mesh convergence and drag force distribution for the UCM model. (a) Mesh convergence and (b) drag force distribution.

mesh HD is extremely slow to reach steady state. To eliminate hundreds of negative eigenvalues without jeopardizing the accuracy, we may need several incremental variations in the artificial damping constant. Although, in principle, this is possible, the cost of computation will be very high with an explicit scheme. It may be faster to get a solution on mesh HD with an implicit time discretization.

Table I provides a detailed comparison between the drag forces predicted using the CBS method and the other available methods. It appears that the CBS method closely agrees with the other methods.

To estimate the impact of the artificial damping on the results, we have plotted the extra stress $\tau_{11}^{p}$ variation with and without artificial damping over the cylinder surface and along the mid-horizontal line in Figure 7. The unstructured mesh A and a Deborah number of 0.3 are used for the comparison. As seen, steep changes in the stress are noted on the surface. The difference in the peak values of the stress with and without damping is apparent. The artificial damping clearly reduces the peak value. However, if the artificial damping is not used, the positive definiteness is



DOI: 10.1002/fld

Table I. Drag force calculated by the fully explicit CBS scheme for Maxwell fluid flow past a circular cylinder.

| *De* | Mesh A | Mesh B | Mesh C | Mesh HD | Fan *et al.* DEVSS | Alves *et al.* M120 SMART |
|---|---|---|---|---|---|---|
| 0.0 | 128.682 | 130.479 | 132.060 | 132.220 | 132.36 | 132.369 |
| 0.01 | 130.694 | 131.646 | 132.058 | 132.105 | | 132.251 |
| 0.025 | | | | | | 131.945 |
| 0.05 | 129.505 | 130.324 | 130.798 | 130.993 | | 130.912 |
| 0.1 | 125.832 | 126.703 | 127.327 | 127.386 | 127.42 | 127.356 |
| 0.2 | 114.924 | 116.628 | | 117.419 | 117.83 | 117.767 |
| 0.3 | 103.217 | 106.874 | | 108.428 | 108.68 | 108.614 |
| 0.4 | 95.345 | 98.881 | 100.828 | 101.074 | 101.43 | 101.361 |
| 0.5 | 90.448 | 93.597 | | 96.567 | 96.11 | 96.037 |
| 0.6 | 88.895 | 92.669 | | 94.182 | 92.37 | 92.298 |
| 0.7 | 90.530 | 90.870 | | 91.751 | 89.84 | 89.774 |
| 0.8 | 94.393 | 90.432 | | | 88.18 | 88.178 |
| 0.9 | | 89.931 | | | | 87.218 |
| 1.0 | | 89.640 | | | | |

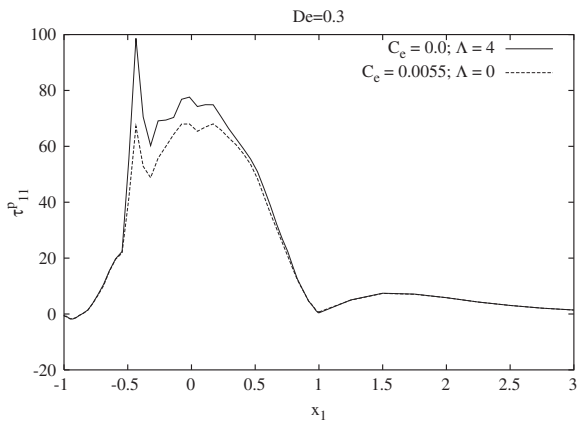


Figure 7. Extra stress $\tau_{11}^p$ distribution over the cylinder and along the mid-vertical centerline, $De=0.3$ (mesh A). Comparison between the distributions with and without artificial damping.

not guaranteed. As given, there are four negative eigenvalues without damping ($C_e=0$). However, when a small amount of artificial damping is added ($C_e=5.5\times10^{-3}$), the negative eigenvalues disappear. It is also obvious that the influence of artificial damping on the stress value in the wake is negligibly small.

Figure 8 shows the extra stress $\tau_{11}^p$ distribution over the cylinder and along the mid-horizontal line for different Deborah numbers using the hybrid mesh HD. The artificial damping is essential to eliminate negative eigenvalues beyond a Deborah number of 0.2. The stress profiles are much smoother than the ones obtained on Mesh A, demonstrating that the finer mesh produces a better solution. It is also noted that the peak value on the cylinder surface starts going down beyond



DOI: 10.1002/fld

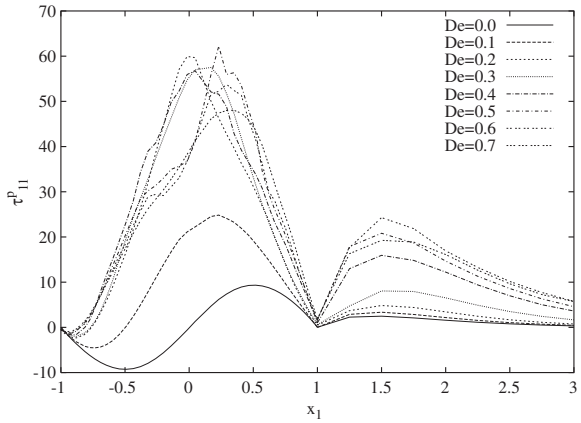


Figure 8. Extra stress $\tau^p_{11}$ distribution over the cylinder and along the mid-vertical centerline for different Deborah numbers (mesh HD).

a Deborah number value of 0.5. This could be the effect of artificial damping. As the Deborah number increases, the demand for artificial damping also increases. The lower peak may be the result of controlled but incorrect artificial damping. Further theoretical research may be necessary to determine an optimal value of damping. A peak value change similar to the one on the cylinder surface is also noted in the wake. However, the peak value here goes down only beyond a Deborah number value of 0.6.

Often it is essential to check the qualitative results to make sure that the solution is smooth. In Figure 9 we show contours of the first normal stress difference $N_1 = \tau^p_{11} - \tau^p_{22}$ and the two components of the extra stresses at $De = 0.7$. Mesh HD was used here to make sure that the solution is as accurate as possible. As seen the solution shows no unphysical oscillations in any part of the domain.

## 5. CONCLUSIONS

In this paper the UCM model was studied using the fully explicit CBS scheme to solve viscoelastic flow over a stationary circular cylinder placed in a rectangular channel. An additional AD method was introduced into the discrete constitutive equations to counteract the negative dissipation. The artificial damping was essential in removing negative eigenvalues of the conformation matrix from the flow domain but AD is not always essential to reach steady state. The results were in close agreement with the published results at lower *De*, and at higher *De* values the deviation is small. In addition to demonstrating that the CBS scheme along with an artificial damping can be an alternative method to solve UCM equations, we have also demonstrated that the *De* limit can be further enhanced with the expense of substantially more computational time. However, a better way of carrying out higher *De* calculations may be via implicit treatment of the constitutive equations using appropriate methods. Implicit matrix-free methods such as GMRES may offer a faster option to solve the constitutive equations. Irrespective of the methods used, the artificial damping introduced will be useful in retaining the positive definitiveness of the problem.



DOI: 10.1002/fld

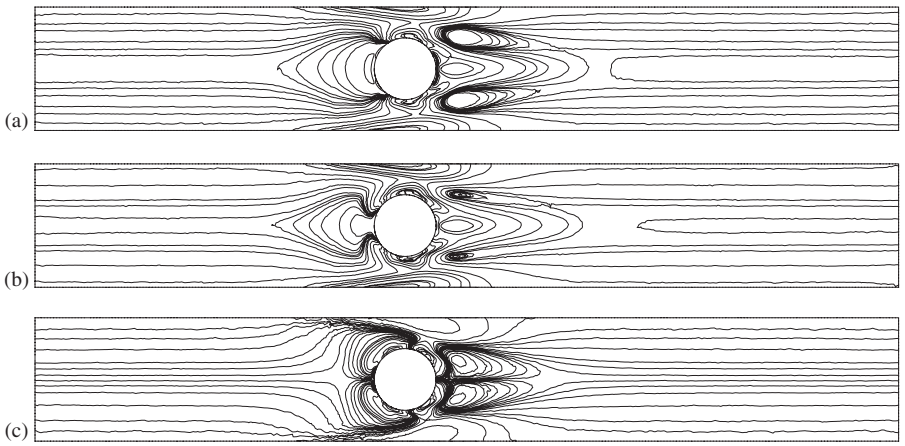


Figure 9. Maxwell fluid flow past a circular cylinder at $De=0.7$, $Re=0.0$ (mesh HD). (a) $N_1$ contours: $N_{1_{\min}}=-12.458$, $N_{1_{\max}}=48.517$; (b) $\tau^p_{11}$ contours: $\tau^p_{11_{\min}}=-0.962$, $\tau^p_{11_{\max}}=48.416$; and (c) $\tau^p_{12}$ contours: $\tau^p_{12_{\min}}=-17.897$, $\tau^p_{12_{\max}}=17.962$.

ACKNOWLEDGEMENTS

This research is funded by the Engineering and Physical Sciences Research Council (EPSRC) grant no. EP/C515498/1.

REFERENCES

1. Nithiarasu P. A fully explicit characteristic based split (CBS) scheme for viscoelastic flow calculations. *International Journal for Numerical Methods in Engineering* 2004; **60**:949–978.
2. Liu CB, Nithiarasu P. The characteristic based split (CBS) method for viscoelastic flow past a circular cylinder. *International Journal for Numerical Methods in Fluids* 2007; DOI: 10.1002/fld.1625.
3. Warichet V, Legat V. Adaptive high-order prediction of the drag correction factor for the upper-convected Maxwell fluid. *Journal of Non-Newtonian Fluid Mechanics* 1997; **73**:95–114.
4. Fan Y. A comparative study of the discontinuous Galerkin and continuous SUPG finite element methods for computation of viscoelastic flows. *Computer Methods in Applied Mechanics and Engineering* 1997; **141**:47–65.
5. Fan Y, Tanner RI, Phan-Thien N. Galerkin/least-square finite-element methods for steady viscoelastic flows. *Journal of Non-Newtonian Fluid Mechanics* 1999; **84**:233–256.
6. Phan-Thien N, Dou HS. Viscoelastic flow past a cylinder: drag coefficient. *Computer Methods in Applied Mechanics and Engineering* 1999; **180**:243–266.
7. Alves MA, Pinho FT, Oliveira PJ. The flow of viscoelastic fluids past a cylinder: finite-volume high-resolution methods. *Journal of Non-Newtonian Fluid Mechanics* 2001; **97**:207–232.
8. Fattal R, Kupferman R. Constitutive laws for the matrix-logarithm of the conformation tensor. *Journal of Non-Newtonian Fluid Mechanics* 2004; **123**:281–285.
9. Hulsen MA, Fattal R, Kupferman R. Flow of viscoelastic fluids past a cylinder at high Weissenberg number: stabilized simulations using matrix logarithms. *Journal of Non-Newtonian Fluid Mechanics* 2005; **127**:27–39.
10. Coronado OM, Arora D, Behr M, Pasquali M. A simple method for simulating general viscoelastic fluid flows with an alternate log-conformation formulation. *Journal of Non-Newtonian Fluid Mechanics* 2007; **147**:189–199.
11. Kim JM, Kim C, Ahn KH, Lee SJ. An efficient iterative solver and high-resolution computations of the Oldroyd-B fluid flow past a confined cylinder. *Journal of Non-Newtonian Fluid Mechanics* 2004; **123**:161–173.
12. Hu X, Ding Z, Lee LJ. Simulation of 2D transient viscoelastic flow using the CONNFFESSIT approach. *Journal of Non-Newtonian Fluid Mechanics* 2005; **127**:107–122.

13. Baaijens FPT. Application of low-order discontinuous Galerkin methods to the analysis of viscoelastic flows. *Journal of Non-Newtonian Fluid Mechanics* 1994; **52**:37–57.
14. Fan Y. Limiting behavior of the solutions of a falling sphere in a tube filled with viscoelastic fluids. *Journal of Non-Newtonian Fluid Mechanics* 2003; **110**:77–102.
15. Grande E, Laso M, Picasso M. Calculation of variable-topology free surface flows using CONNFFESSIT. *Journal of Non-Newtonian Fluid Mechanics* 2003; **113**:127–145.
16. Coronado OM, Arora D, Behr M, Pasquali M. Four-field Galerkin/least-squares formulation for viscoelastic fluids. *Journal of Non-Newtonian Fluid Mechanics* 2006; **140**:132–144.
17. Zienkiewicz OC, Codina R. A general algorithm for compressible and incompressible flow—part I: the split, characteristic-based scheme. *International Journal for Numerical Methods in Fluids* 1995; **20**:869–885.
18. Zienkiewicz OC, Nithiarasu P, Codina R, Vázquez M, Ortiz P. The characteristic-based-split procedure: an efficient and accurate algorithm for fluid problems. *International Journal for Numerical Methods in Fluids* 1999; **31**:359–396.
19. Zienkiewicz OC, Taylor RL, Nithiarasu P. *The Finite Element Method for Fluid Dynamics* (6th edn). Elsevier: Amsterdam, 2005.
20. Nithiarasu P. An efficient artificial compressibility (AC) scheme based on characteristic based split (CBS) method for incompressible flows. *International Journal for Numerical Methods in Engineering* 2003; **56**:1815–1845.
21. Nithiarasu P, Mathur JS, Weatherill NP, Morgan K. Three dimensional incompressible flow calculations using the characteristic based split (CBS) scheme. *International Journal for Numerical Methods in Fluids* 2004; **44**:1207–1229.
22. Nithiarasu P. An arbitrary Lagrangian–Eulerian (ALE) method for free surface flow calculations using the characteristic based split (CBS) scheme. *International Journal for Numerical Methods in Fluids* 2005; **48**: 1415–1428.
23. Nithiarasu P, Liu CB. An artificial compressibility based characteristic based split (CBS) scheme for steady and unsteady turbulent incompressible flows. *Computer Methods in Applied Mechanics and Engineering* 2006; **195**:2961–2982.
24. Nithiarasu P, Zienkiewicz OC. Analysis of an explicit and matrix free fractional step method for incompressible flows. *Computer Methods in Applied Mechanics and Engineering* 2006; **195**:5537–5551.
25. Nithiarasu P, Codina R, Zienkiewicz OC. The characteristic based split (CBS) scheme—a unified approach to fluid dynamics. *International Journal for Numerical Methods in Engineering* 2006; **66**:1514–1546.
26. Nithiarasu P, Liu CB, Massarotti N. Laminar and turbulent flow through a model human upper airway. *Communications in Numerical Methods in Engineering* 2007; **23**:1057–1069.
27. Peraire J, Peiro J, Formaggia L, Morgan K, Zienkiewicz OC. Finite element Euler computations in three dimensions. *International Journal for Numerical Methods in Engineering* 1988; **26**:2135–2159.
28. Morgan K, Peraire J, Peiro J, Zienkiewicz OC. Adaptive remeshing applied to the solution of a shock interaction problem on a cylindrical leading edge. In *Computational Methods in Aeronautical Fluid Dynamics*, Stow P (ed.). Clarendon Press: Oxford, 1990; 327–344.
29. Peraire J, Peiro J, Morgan K. Multigrid solution of the 3-D compressible Euler equations on unstructured tetrahedral grids. *International Journal for Numerical Methods in Engineering* 1993; **36**:1029–1044.
30. Nithiarasu P, Zienkiewicz OC, Satya Sai BVK, Morgan K, Codina R, Vázquez M. Shock capturing viscosities for the general fluid mechanics algorithm. *International Journal for Numerical Methods in Fluids* 1998; **28**: 1325–1353.
31. Hassan O, Sorensen KA, Morgan K, Weatherill NP. A method for time accurate turbulent compressible fluid flow simulation with moving boundary components employing local remeshing. *International Journal for Numerical Methods in Fluids* 2007; **53**:1243–1266.
32. Marchal JM, Crochet MJ. A new mixed finite element for calculating viscoelastic flow. *Journal of Non-Newtonian Fluid Mechanics* 1987; **26**:77–114.
33. Lozinski A, Owens RG. An energy estimate for the Oldroyd B model: theory and applications. *Journal of Non-Newtonian Fluid Mechanics* 2003; **112**:161–176.



DOI: 10.1002/fld